Noise and Performance of a Counter-Rotation Propeller

S. Fujii,* H. Nishiwaki,† and K. Takeda†
National Aerospace Laboratory, Chofu, Tokyo, Japan

The noise and aerodynamic performance of a 3×3 counter-rotating propeller scale model were quantified experimentally in anechoic environments with a velocity of 68 m/s incoming flow on. The model diameter was 400 mm and the aft blade rotational speeds and the rotational Mach numbers were varied up to 9000 rpm and 0.55, respectively, while the front blades were kept at 9000 rpm. The reinforcement of counter-rotating harmonics was observed even at high blade passage frequencies. The axial separation between two rotors had a favorable effect on the noise levels, whereas an adverse effect on the performance was found for the large spacing with axial velocity acceleration attendant. The spike due to the overturning of tangential velocity was found near the tip section. A difference of the rotational speeds yielded the spinning sound waves with a beat frequency of three times the rps difference. The split frequencies could be identified on the measured spectrum when the two rotors had such nonsynchronous rotational speeds.

Nomenclature

A = area
B = number of blades
D = diameter of propeller
f = frequency
H = enthalpy or total head
I = rothalpy
J = advance ratio
k = load harmonic
ℓ = axial spacing between two rotors
M = Mach number
m = sound harmonic
N = rotational speed
P = pressure
r = radius
s = static
T = thrust
t = total
U = axial velocity
W = tangential velocity
Ω = angular velocity
β = blade setting angle
ρ = density
∞ = downstream infinity

Subscripts

0 = in front of first propeller
1 = after first propeller or front blade
2 = in front of second propeller or aft blade
3 = after second propeller
T = tip

Introduction

THE configuration of counter-rotating propellers has a great potential as fuel conservative propulsors.[1] The efficiency advantage can be offered by counter-rotation (CR) to minimize swirl losses.[2] The aerodynamic and acoustic interaction between two rotors may give rise to rather complex phenomena. Recently, the CR noise theory was recast by Hanson.[3] The objective of the present paper is to determine experimentally the noise and aerodynamic performance of a CR propeller scale model under aircraft takeoff and landing conditions and to gain a more fundamental understanding of the interaction phenomena. The tests were carried out under the same conditions as those previously reported[4] in anechoic environments with incoming low-speed flow from a duct.

Received Feb. 4, 1986; revision received April 30, 1986.

*Head, Engine Noise Group.
†Senior Researcher, Engine Noise Group.

Test Facilities and Instrumentation

The drive system for the rear blades consisted of the same blades and the same test rig as those used previously.[4] The front drive system was newly manufactured and is shown in Fig. 1. The front blades were driven by a set of gears and a 50 kW air-cooled electric motor, which had a constant rotational speed of nearly 9000 rpm and a rotational tip Mach number of 0.55. The exact rpm depended on the blade loading. The 75 kW water-cooled electric motor for the rear blades could be varied from 1000 to 9000 rpm. The front blades had the same profile as the rear blades and they were mirror images of each other. The 400 mm diam scale-model CR propellers were placed in a $3.0\times5.5\times8.5$ m^3 anechoic chamber with a 650 mm diam duct that provided a maximum flow velocity up to 68 m/s at the front propeller disk. The number of blades was a 3×3 CR system with the 27 deg swept angle at the tip section. The vertical strut, which was shaped as the symmetrical airfoil and housed one of the front drive shafts, produced the wake at the first propeller disk. The wake circumferential width and velocity deficit were $d/\pi D=0.048$, $u/U\infty=0.92$, respectively, for $U\infty=68$ m/s. The axial spacing between two rotors was changed by sliding the front drive rig on rails. A lightweight hollow cylinder was attached to the rear propeller spinner to minimize the gap between the front and rear shaft hubs. The present configuration was therefore considered the rear-mount pusher CR model.

An array of 12.5 mm diam condenser microphones was placed outside the jet flow at a distance of 2.5 m from the middle point of the front and aft propeller disks and at the same height as the shaft axis. The other array of microphones was circled around the CR blade system at a distance of 1.4 m to determine the circumferential lobe pattern of the sound pressure. Care was taken to muffle most of the test rig surfaces with urethane foam to minimize the sound reflection. In the previous single-rotation tests,[4] it was guaranteed that the noise data without any modification due to the jet edge shear could be obtained up to a duct-flow velocity of 30 m/s. However, for the CR test system, there occurred asymmetric inlet distortion with such a slow incoming velocity. Therefore, the acoustic measurements were made only at a velocity of 68

m/s to avoid the distortion, which makes the noise generation complex and is beyond the scope of the present report. It should be understood that a possible effect of shear layer on the noise data exhibited in the following would be inevitably included. All data were handled through the NAL on-line noise reduction system.

The measurement of thrust and torque through the rotating-shaft strain gages was not realized in the front propeller system due to structure complexities, although it was done in the rear propeller. Therefore, the flow data obtained from the three-hole pitot tube traverses was used to compute the thrust by the relationship[5] $dT=(Ps\infty/PT\infty)^{5/7}(Pt-Pt\infty)dA$. The torque for the front blades was based on the electric current and voltage readings in the driving motor. By use of the aft shaft system it was calibrated that the values by such procedures gave rise to $\pm 10\%$ deviation from those by the strain gage method. The CR system is shown in Fig. 2. The microphone arrays and aerodynamic traverse directions are illustrated in Fig. 1. The noise and flow survey was made independently.

Noise Data and Discussion

A typical example of the sound pressure spectrum for the CR propellers is demonstrated in Fig. 3. Although a rapid decrease of the second and third harmonics occurred in the single rotation,[4] the appearance of many harmonics up to the eleventh in the CR resembled the sound signature observed in the turbofan engine, where the wakes shed from the fan rotor interacted with the stator vanes. The reinforcement of counter-rotating harmonics was also reported in the airfoil shank tests.[6] For the same blade numbers and rpm on both rotors, all frequencies are multiples of blade passage frequency (BPF) of one of the rotors (Fig. 3). The effect of axial spacing between two rotor disks on the spectrum is shown in comparison in Figs. 3 and 4. A considerable decay of sound pressure levels was detected in each BPF when the spacing was large. Little change in the first harmonic was observed only for the side line; at other angles a decrease of 2-3 dB was obtained even for the first BPF.

At the same blade angle as that in Fig. 3, the rpm of aft blades and rotational tip Mach number were set at 7980 rpm and $M_T=0.49$ while the front blades were driven at 9100 rpm and $M_T=0.55$. The result is shown in Fig. 5. For the general case with blade numbers and rpm not necessarily the same on both rotors, all of the frequencies can be heard in $|mB_2N_2+kB_1N_1|$, using the rear rotor as the reference, as was fully explained by Hanson.[3] By use of this formula, the frequencies of many spikes on the spectrum were evaluated in Table 1. The first four groups denoted as a and b were chosen and attempted to identify the corresponding frequencies on the measured data of Fig. 5. However, all designated frequencies were not necessarily recognized probably because some of them had very weak pressure levels.

A difference of rpm between two rotors may have an effect of interest on the sound pressure field as a result of the acoustic interaction. Fig. 6 shows a relationship obtained from decreasing slightly the aft blade rotational speeds. The beat frequency had three times the rps difference frequency $(N_1-N_2)/60$ rps. The amplitude in beating was increased as the rps difference became small.

The seven microphones, circled around the axis at a point midway between the two rotor disks, produced part of the circumferential pattern of sound pressure, (Fig. 7). This blade rotates slowly with a frequency of $3(N_1-N_2)/60$ rps in the same direction as that of the faster front blade rotation. For the synchronous CR propeller $N_1=N_2$, we should expect the standing wave pattern. Since the circumferential mode orders are given by $(m-2k)B$, the pattern seen to the observer is the result of summing them up for m and k on all integer values from $-\infty$ to $+\infty$. For the even numbers of $m=2, 4, 6\ldots$, the zero-order modes of high radiation efficiency may be generated. The trends of the overall sound pressure levels with

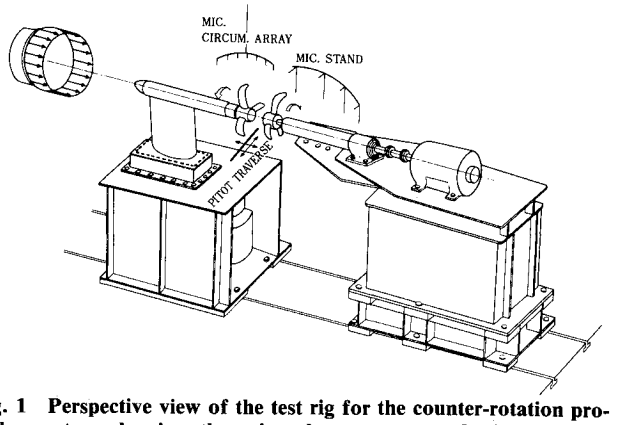

Fig. 1 Perspective view of the test rig for the counter-rotation propeller system showing the microphone arrays and pitot traverse directions.

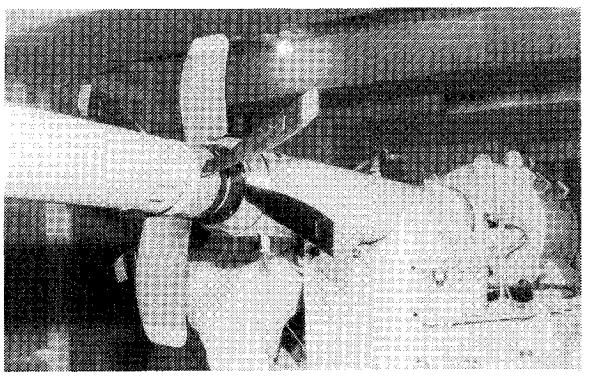

Fig. 2 3×3 CR scale-model and drive motor for the rear blades.

Table 1 Calculated values of $|mBN_2+kBN_1|$ for $N_2=7980$ rpm, $M_T=0.49$, $N_1=9100$ rpm, $M_T=0.56$, $B=3$ for the first four clusters

Sound harmonic m	Load harmonic k	Frequency f, Hz	Group I	II	III	IV
1	−1	46				
	0	399	a			
	1	854		b		
	2	1329			c	
	3	1764				d
2	−1	353	a			
	0	798		b		
	1	1253			c	
	2	1688				d
	3	2154				
3	−1	752		b		
	0	1197			c	
	1	1642				d
	2	2097				
	3	2542				
	4	2987				
4	−1	1151			c	
	0	1596				d
	1	2041				
	2	2496				
	3	2951				
	4	3406				
	5	3861				
0	−1	455	a			
	1	455				
	2	910		b		
	3	1365			c	
	4	1820				d

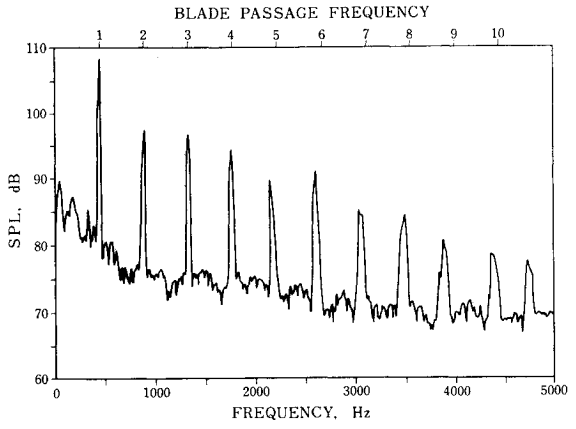

Fig. 3 Narrow-band sound-pressure-level spectra for the CR propellers with small disk spacing: $\beta_1 = 36$ deg, $\beta_2 = 36$ deg, $N_1 = N_2 = 9000$ rpm, $M_T = 0.55$, $U\infty = 68$ m/s, $\ell/D = 0.2$.

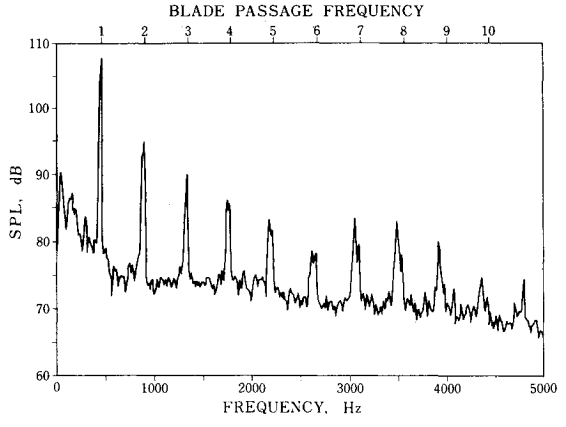

Fig. 4 Narrow-band sound-pressure-level spectra for the CR propellers with large disc spacing: $\beta_1 = 36$ deg, $\beta_2 = 36$ deg, $N_1 = N_2 = 9000$ rpm, $M_T = 0.55$, $U\infty = 68$ m/s, $\ell/D = 0.4$.

the variation of the aft blade rotational tip Mach number as well as blade angles are compared in Fig. 8. The effect of axial spacings also is shown for the blade angle of $\beta_1 = \beta_2 = 36$ deg. The maximum sound level obtained for the case with $\beta_1 = \beta_2 = 39$ deg, which produced the highest thrust and the measured velocity triangles, are illustrated in Fig. 9.

The Flow Data

In the case with a large axial-spacing of $\ell/D = 0.40$, the pitot tube traverse data was presented to show the flow behavior in the intradisk region between the two rotors, (Fig. 10). The negligible change of tangential velocity in passing the large spacing suggests that no appreciable radial-shift of the streamlines occurred because the angular momentum, (tangential velocity) × (streamline radius), was kept constant because there was no external force imposed on each of the axisymmetric streamlines. The axial velocity was increased toward the front of the aft blades, which reflected a reduction in the static pressure and density by considering the conservation of mass flow, although the data was not figured herein. The detailed comparisons of tangential velocity, axial velocity, and total pressure ratio at the exit of the second propeller are shown in Figs. 11-13 for the small and large spacings. The tangential velocity was turned over into the direction of the second propeller rotation near the root and tip for the small spacing with $N_2 = 9000$ rpm, $M_T = 0.55$ (Fig. 11). The spike due to the overturn of tangential velocity near the tip section was predominant as the spacing became large. The same phenomenon, which might be caused by the tip vortex and was

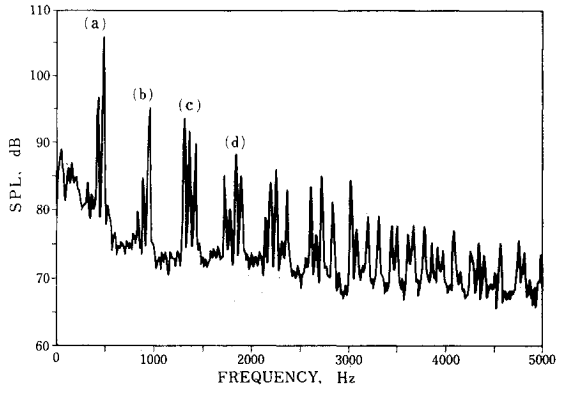

Fig. 5 Narrow-band sound-pressure-level spectra for the CR propellers with different rotational speeds: $\beta_1 = 36$ deg, $\beta_2 = 36$ deg, $N_1 = 9100$ rpm, $M_T = 0.56$, $N_2 = 7980$ rpm, $M_T = 0.49$, $U\infty = 68$ m/s, $\ell/D = 0.2$.

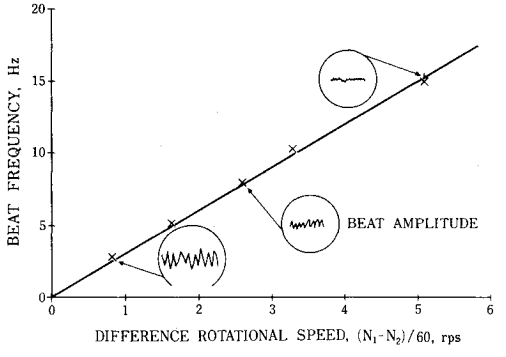

Fig. 6 Beat frequency of the sound pressure interaction by a pair of propellers: $N_1 = 9100$ rpm, $M_T = 0.56$, $U\infty = 68$ m/s.

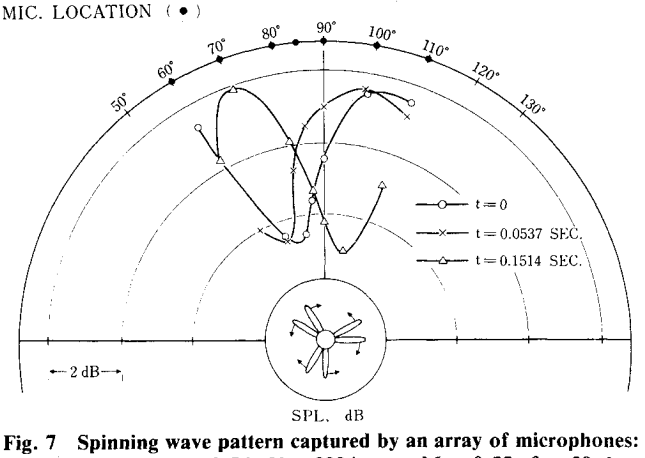

Fig. 7 Spinning wave pattern captured by an array of microphones: $N_1 = 9080$ rpm, $M_T = 0.56$, $N_2 = 8994$ rpm, $M_T = 0.55$, $\beta_1 = 39$ deg, $\beta_2 = 36$ deg, $U\infty = 68$ m/s.

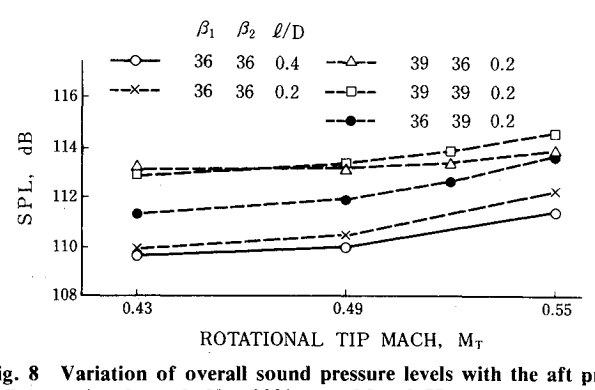

Fig. 8 Variation of overall sound pressure levels with the aft propeller rotational speed: $N_1 = 9000$ rpm, $M_T = 0.55$, $U\infty = 68$ m/s.

not evident on the single-rotation data,[4,7] was already pointed out by Dunham et al.[7] The simplified analysis of a two-dimensional flow model is made in the Appendix. As Eq. (A6) indicates, the static pressure change, or implicitly the thrust, is increased by the total pressure rise and decreased by the axial velocity acceleration and swirl loss. With this in mind, a comparison of Figs. 12 and 13, the total pressure ratio was larger with smaller values of axial velocity acceleration in the same spacing case. This was the favorable result that increased the thrust in considering Eq. (A6). In fact, the measured overall thrust was 10% higher in the present small spacing configuration. It was then revealed that the large spacing had an adverse effect on the aerodynamic performance. In other words, the redistribution of the static pressure and, hence, axial velocity due to the presence of large spacing, reduced the aerodynamic, advantage of the CR system. It can be said that the negative thrust produced by the axial acceleration would be minimized by making the spacing as small as possible. This is in contrast with the acoustic standpoint; the noise level decays as the axial separation becomes large.

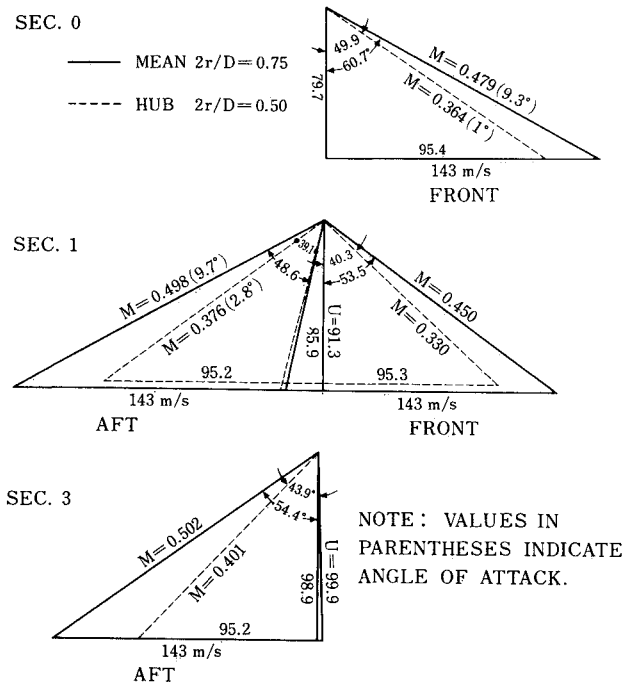

Fig. 9 Velocity triangles at the root and mean sections, $\beta_1=\beta_2=39$ deg, $N_1=N_2=9000$ rpm, $M_T=0.55$, $U\infty=68$ m/s.

As for the minimum practical clearance of $\ell/D=0.20$, the effects of the front and aft blade setting angle on the thrust and efficiency were quantified in Figs. 14 and 15. As expected, the change of blade setting angle in the rear propeller gave very little impact on the front rotor performance while the front blade setting angle had the dominant influence over the rear propeller aerodynamics. In Fig. 14, the values of thrust and efficiency of the rear propeller were lower than those of the front propeller even at $\beta_1=\beta_2=39$ deg. To obtain equal thrust it was necessary to increase either the rotational speed or the blade setting angle of the rear rotor, but neither was possible due to the mechanical constraints of the test rig. A thorough check of the measured data indicates that the angles of attack to the second propeller were significantly low, down to 3 deg at the root section, which led to the aft-rotor poor efficiencies, as indicated in Fig. 9. At $\beta_1=30$ deg, the angles of attack approached the design values along the whole span of the second rotor by which the efficiency in the second propeller increased up to the value of the first propeller, Fig. 15. Note that the efficiency was adversely affected by reductions of the aft rpm at the blade setting angles providing the equally absorbed power of both rotors in the unsteady analysis.[8] As the two rotors had mirror images of each other in their blade profiles, the increase of the axial velocity across the first propeller had a tendency to make the attack angle smaller than the design in the second propeller. The same thrust and efficiency

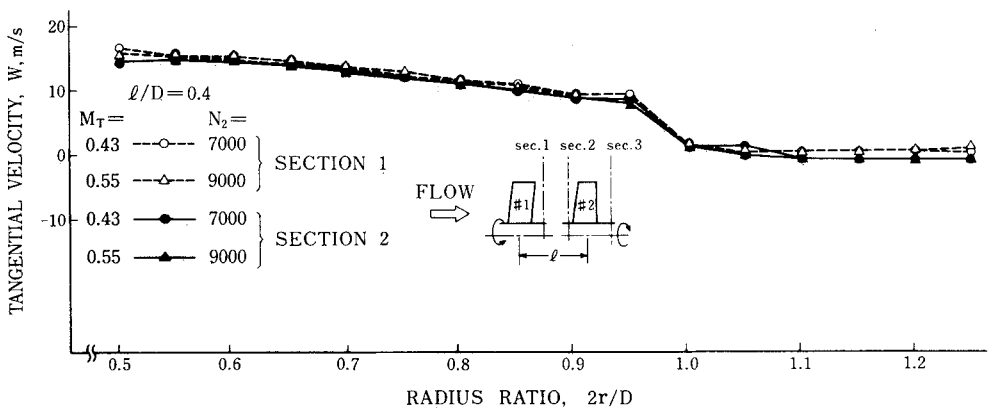

Fig. 10 Tangential velocity distribution at sections 1 and 2: $\beta_1=\beta_2=36$ deg, $N_1=9000$ rpm, $M_T=0.55$, $U\infty=68$ m/s.

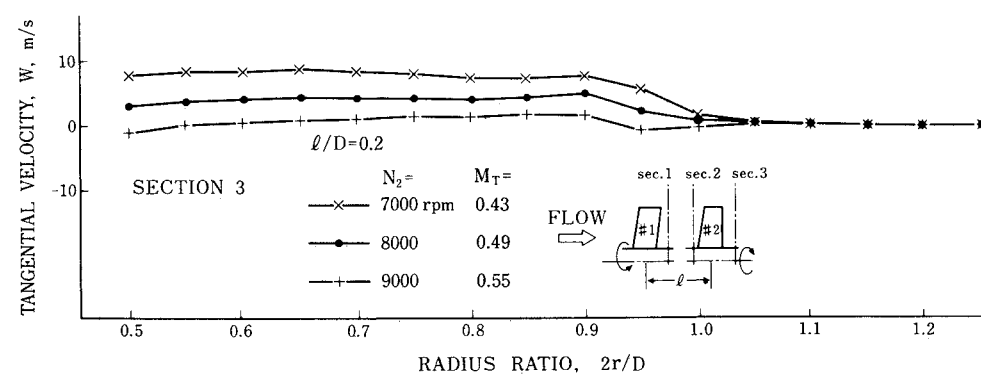

Fig. 11 Tangential velocity at exit of second propeller, section 3, for small spacing: $\beta_1=\beta_2=36$ deg, $N_1=9000$ rpm, $M_T=0.55$, $U\infty=68$ m/s.

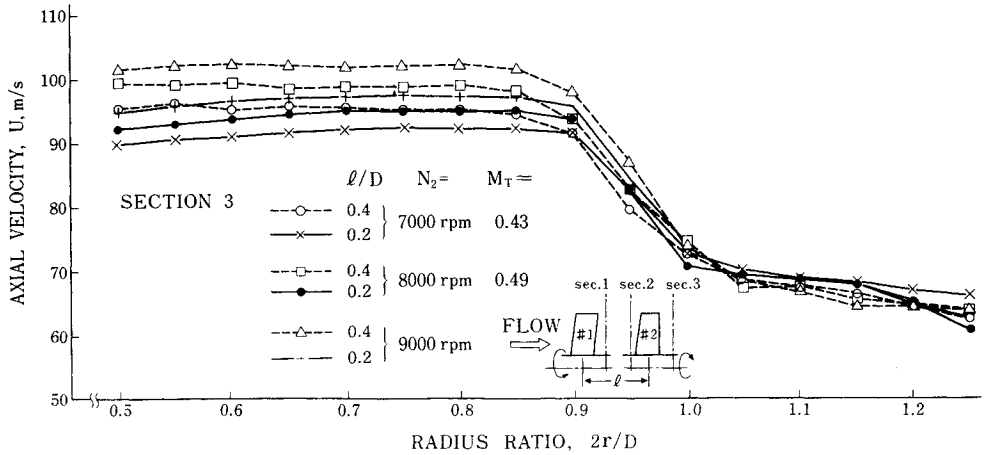

Fig. 12 Axial velocity distribution at section 3 for small and large spacings: $\beta_1 = \beta_2 = 36$ deg, $N_1 = 9000$ rpm, $M_T = 0.55$, $U\infty = 68$ m/s.

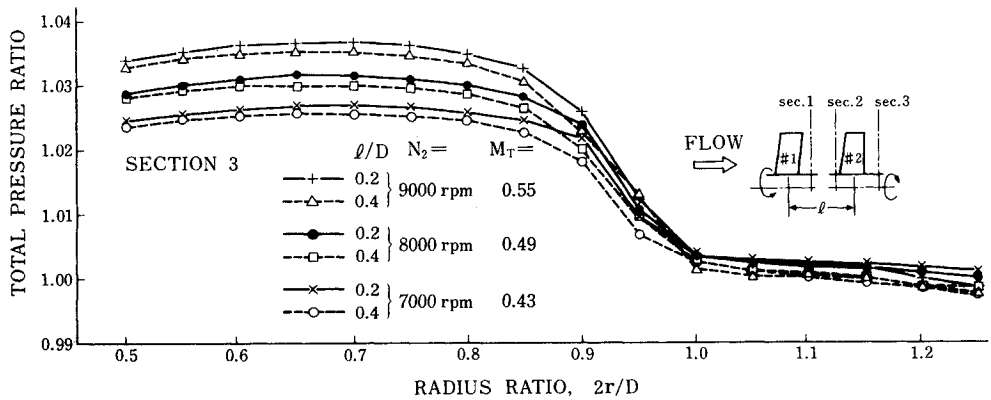

Fig. 13 Total pressure ratio across CR propellers for small and large spacings: $\beta_1 = \beta_2 = 36$ deg, $N_1 = 9000$ rpm, $M_T = 0.55$, $U\infty = 68$ m/s.

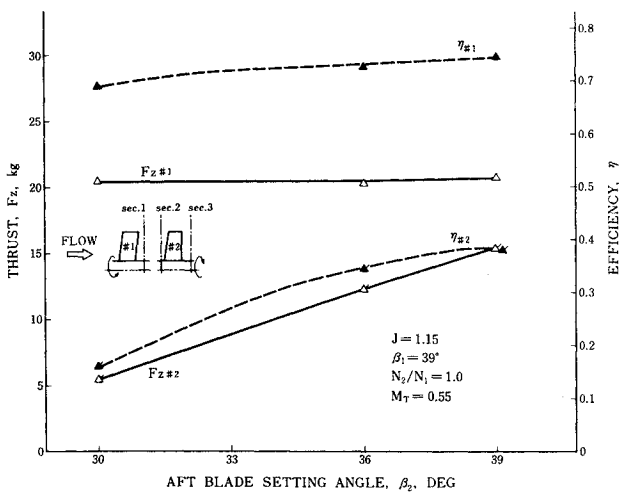

Fig. 14 Thrust and efficiency variations with aft blade angles at $\beta_1 = 39$ deg, $N_1 = 9000$ rpm, $M_T = 0.55$, $U\infty = 68$ m/s.

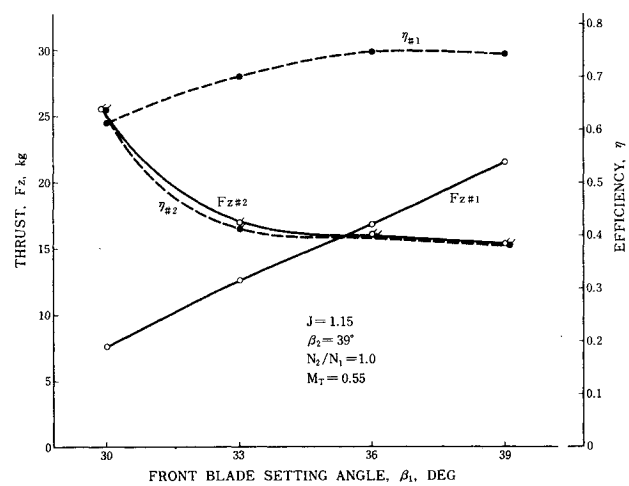

Fig. 15 Thrust and efficiency variations with front blade angles at $\beta_2 = 39$ deg, $N_1 = 9000$ rpm, $M_T = 0.55$, $U\infty = 68$ m/s.

on the two rotors were not realized under the present conditions.

The three dimensionality and various operating conditions in the wide range from the takeoff to the cruise speeds would make it difficult to meet every requirement of the flow angles in the second blade inlet along the whole span. The detailed flow calculations are needed at the design and off-design conditions in advance for maximizing or compromising aerodynamic efficiency without the expense of hardware building as has been frequently been done in the multistage turbomachinery. Furthermore, it is important to have the data on the adequate pitch angles of both propellers at different operating points. The CR is taken to be a compressor or fan stage, where the noise and thrust are generated as if the stator vanes were rotating with the outer walls removed.

Conclusions

The interaction phenomena of a 3×3 counter-rotation scale model were experimentally determined under takeoff and landing conditions in anechoic environments. The spacing between two rotors, the rotational speeds of the aft propeller, and the blade setting angles of both rotors were the experimental parameters chosen. The configuration of the present test rig was the rear-mount pusher model.

It was revealed that a reinforcement of counter-rotating harmonics occurred, which did not decay even at high blade passage frequencies. The favorable effect of axial separation between two rotors on the sound levels was quantified in comparisons of small and large spacing cases. For the blade numbers and rotational speeds not the same on both rotors, all

heard frequencies could be evaluated by use of $(mN_2 + kN_1)B$, except for some undetectable frequencies, probably due to their weakness in sound intensity. It was found that a difference of rotational speeds between two rotors gave rise to the spinning sound waves, which rotated slowly with a speed of $3 \times (N_1 - N_2)/60$ rps. The beat amplitude became large as the rps difference approached zero value.

The large axial spacing had the adverse effect on the aerodynamic performance with the axial velocity acceleration attendant. The spike due to the overturn of tangential velocity near tip sections might be caused by the tip vortex and was not evident in the single rotation data. It was reconfirmed that the possible thrust in the counter rotation was increased by making the axial velocity acceleration as small as possible without swirling components.

Appendix: A Note on Aerodynamics

We assume the incompressible flow through coaxial propellers and ignore the convergence of the flow between them for the sake of simplicity. Then, the total enthalpy H and rothalpy I can be identified as the absolute and relative total pressure. The pressure change across the first propeller is given by

$$H_1 - H_0 = (P_1 - P_0) + \rho(U_1^2 - U_0^2)/2 + \rho W_1^2/2 \quad \text{(A1)}$$

$$I_1 - I_0 = (P_1 - P_0) + \rho(U_1^2 - U_0^2)/2 + \rho(W_1^2 - 2W_1\Omega_1 r_1)/2 \quad \text{(A2)}$$

If there are zero losses due to the friction and secondary flow in the blade passage, we have $I_1 - I_0 = 0$ and, hence, equating the static pressure terms in Eqs. (A1) and (A2) yields

$$H_1 - H_0 = \rho\Omega_1 r_1 W_1 \quad \text{(A3)}$$

This is the well-known Euler's turbine equation. Most of the energy addition given by Eq. (A3) may be used to gain the thrust. A relationship is obtained from Eqs. (A1) and (A3) in addition to the static pressure that has recovered to the free-stream value $(P_1 - P_0)\infty = 0$ at the downstream infinity, such that

$$(U_1 - U_0)\infty = [2(H_1 - H_0)/\rho - W_1^2]/(U_1 + U_0)\infty \quad \text{(A4)}$$

For the second propeller it is written that

$$H_3 - H_1 = \rho\Omega_2 r_2(W_1 - W_3) \quad \text{(A5)}$$

and across the contradisks, the pressure rise is given by

$$P_3 - P_0 = (H_3 - H_0) - \rho(U_3^2 - U_0^2)/2 - \rho W_3^2/2 \quad \text{(A6)}$$

The static pressure rise may be directly correlated to the thrust in the wake suction region near the propeller disk. In Eq. (A6) the dynamic pressure increase including the swirl part must be subtracted from the total pressure addition $(H_3 - H_0)$. It is important to have the minimum values of axial acceleration as well as swirl velocity in order to increase the thrust. At the far downstream, it is written by use of the condition $P_3 - P_0 = 0$ that

$$(U_3 - U_0)\infty = [2(H_3 - H_0)/\rho - W_3^2]/(U_3 + U_0)\infty \quad \text{(A7)}$$

or in terms of the angular rotational velocity explicitly, we have

$$(U_3 - U_0)\infty = [\Omega_1 r_1 W_1 + \Omega_2 r_2(W_1 - W_3) - W_3^2]/(U_3 + U_0)\infty \quad \text{(A8)}$$

As Eqs. (A7) or (A8) stands, the swirling energy loss W_1^2 is cancelled out in the CR equation and the possible maximum value of axial acceleration may be obtained by putting $W_3 = 0$, since it is not practical to make negative the value of W_3. The ideal energy addition by a pair of propellers is therefore

$$H_3 - H_0 = 2\rho\Omega r W_1, \quad (U_3 - U_0) = 2\Omega r W_1/(U_3 + U_0)\infty \quad \text{(A9)}$$

where $\Omega_1 - \Omega_2 - \Omega$, $W_3 = 0$.

Acknowledgment

The Environment Protection Agency of Japan is gratefully acknowledged for its financial support of this study.

References

[1]Strack, W. C., Knip, G., Weisbrich, A. L., Godston, J., and Bradley, E., "Technology and Benefits of Aircraft Counter Rotation Propellers," NASA TM-83983, 1982.

[2]McCutchen, C. W., "A Theorem on Swirl Loss in Propeller Wakes," *Journal of Aircraft*, Vol. 22, April 1985, pp. 344-346.

[3]Hanson, D. B., "Noise of Counter-rotation Propellers," *Journal of Aircraft*, Vol. 22, July 1985, pp. 609-617.

[4]Fujii, S., Nishiwaki, H., and Takeda, K., "Aeroacoustics of an Advanced Propeller Design Under Take-Off and Landing Conditions," *Journal of Aircraft*, Vol. 23, Feb. 1986, pp. 136-141.

[5]Vogeley, A. W., "Flight Measurements of Compressibility Effects on a Three-Blade Thin Clark Y Propeller Operating at Constant Advance-Diameter Ratio and Blade Angle." NASA WR L-505, 1943.

[6]Korkan, K. D., Cornell, C. C., and Camba, J. III, "Experimental Study of Noise Generated by Counterrotating Propeller Systems," AIAA Paper 84-2264, Oct. 1984.

[7]Dunham, D. M., Sellers, W. L. III, and Elliott, J. W., "Laser Velocimeter Measurements of the Flow Fields Around Single- and Counter-Rotation Propeller Models," SAE Paper 850870.

[8]Lesieutre, D. J. and Sullivan, J. P., "The Analysis of Counter-Rotating Propeller Systems," SAE Paper 850869, April 1985.